Journal of Physics: Conference Series

PAPER • OPEN ACCESS

Air preheating potential with high Opaque Ventilated Façade under natural and forced convection

Air preheating potential with high Opaque Ventilated Façade under natural and forced convection

T Colinart[1], H Noel[1], M Batard[1], A Fuentes[1], A Magueresse[1] and P Glouannec[1]

[1] Univ. Bretagne Sud, UMR CNRS 6027, IRDL, Lorient, France

thibaut.colinart@univ-ubs.fr

Abstract. Opaque ventilated façades (OVF) are increasingly used in building envelope because of their positive impact on building energy efficiency. Usually, air flow is driven by natural ventilation. Recently, there were some attempts to drive air flow mechanically to preheat or precool air in combination with HVAC, Heat pump or Latent Heat Thermal Energy Storage (LHTES) systems. In this framework, an experimental real-scale module of an OVF was built (1.9 m width and 3.5 m height). In this study, OVF is tested during autumn under natural and under forced convection by means of ventilator placed at cavity outlet. Inlet air flowrate are changed from day to day or during the day. For each test, temperature, air velocity, air flow rate and thermal flux are monitored at different locations of OVF. Their analysis shows that collector efficiency and amount of collected energy depend mainly on cavity air flow rate. The measurements are compared to simulation results obtained from two thermal models describing OVF: Trnsys Type 1230 and home-developed pseudo 2D. A good agreement is found for air temperature at cavity outlet while differences are observed in opaque layers due to modelling assumptions. Last, sensitivity analysis on two design parameters is carried out.

1. Introduction

Opaque ventilated façade (OVF) consists of an opaque overlaying outer surface separated from the rest of the wall, creating thus a cavity. Because of large design flexibility, OVF is increasingly used in new or renovated building envelope. In the last decade, numerous studies aimed to evaluate its thermal and energy performance [1]. For instance, OVF can reduce thermal load and summer overheating because of the shading effect of outer layer and of the cooling effect induced by air cavity ventilation [2-5]. In winter the benefit of OVF to reduce heat loss through the envelope is questionable [1,6]. On the other hand, recent studies focused on the possibility to transfer absorbed solar energy into the building to reduce heating loads. By directly blowing air preheated in the cavity into the building, Peci Lopez et al. [7] predicted that heating energy consumption can be reduced up to 60 % punctually. Nevertheless, no information on blowing temperature is available, even though it is found that temperature at cavity outlet may reach 40 to 50 °C even in winter [8-9]. Alternatively, OVF can directly integrate latent heat thermal energy systems in the cavity [10] or be coupled with active systems (like heat pump [11]). Recently, some attempts investigated the possibility of coupling OVF with PCM air heat exchanger [12-13]. In the view of assessing air preheating potential (in terms of temperature and energy), this work aims to evaluate experimentally and numerically the thermal performance of a high height OVF prototype.

2. Experiments on OVF

2.1. Experimental set-up

The tested façade presented in figure 1 is built as follow. Horizontal liner trays filled with 10 cm mineral wool insulation and covered by 6 mm radiant barrier (acting also as airtight rainscreen) are fixed on a frame with dimension of 3.5 m × 1.9 m. Four cm thick steel battens are mounted vertically to support black metal cladding with horizontal trapezoidal profile, creating thus 3 ventilation cavity channels. A plenum was sealed on the top to collect warmed air. When tested under forced convection, a 3 m flexible duct and a fan are connected to the plenum outlet.

A series of sensor and devices is used to monitor the thermal behavior of the central part and the right side of the wall (see figure 1). Temperature is measured with K-thermocouples (nominal accuracy ± 0.25 K) at cladding surface, within cavity (not shielded from radiation) and across radiant barrier at different positions. Additional K-thermocouples are in the plenum outlet. Heat flux sensors (Captec, nominal uncertainty ± 3 %) are placed behind the radiant barrier at three different locations. Air velocity is measured at the middle of ventilated channels by means of two hot wire anemometers (TSI 8465, nominal uncertainty ± 2 %). In addition, volumetric flow rate q_v^{air} is measured directly in the plenum outlet with vane anemometer (Kimo SVH-100, nominal uncertainty ± 3 %). Outdoor conditions at the wall vicinity are also recorded. Global solar irradiation E_s is measured on the upper part of the wall with one pyranometer (Kipp and Zonen CMP10) aligned with the tested wall. K-thermocouples are used to measure temperature at the cavity inlet and at the mid-height of the wall and behind it. A cup anemometer is set up at the front of the wall to measure the wind velocity v_{wind}. None of the sensors or mountings shaded the panel. Note that long-wave radiation from the environment was not measured. All sensor signals are recorded by dataloggers with one minute time step.

The set-up is mobile and can be tilted. In the present work, the vertically tilted wall oriented in SSE direction is tested in the campus of Université Bretagne Sud (Lorient, France). Four experiments are performed during four separate days in November 2020, two under natural convection and two under forced convection. Each experiment lasts only 4h (from 10am to 2pm) because of shadow caused by other buildings. Mean weather conditions are gathered in Table 1.

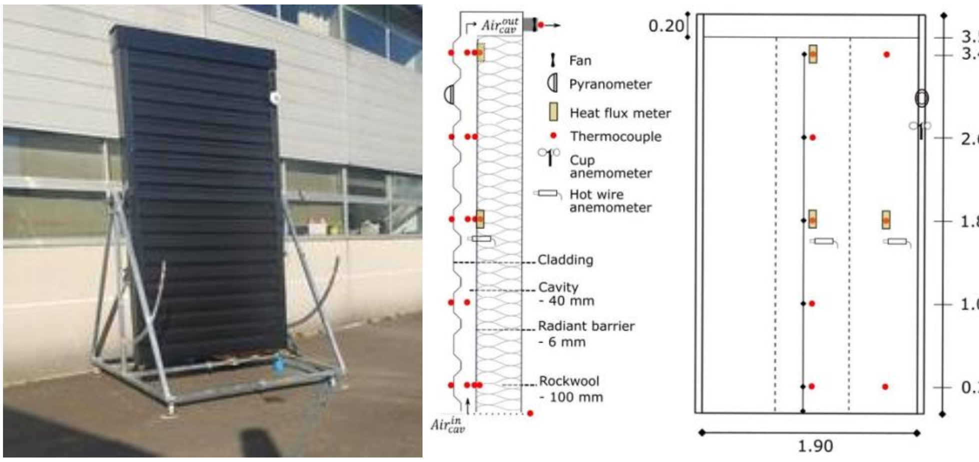

Figure 1. View of the experimental set-up and of its instrumentation.

2.2. Experimental results

The first natural convection experiment is performed under ideal sunny autumn conditions: clear sky conditions (solar irradiation ideally parabolic), monotone increase of exterior temperature from 9 to 15 °C and constant wind velocity. Under these conditions, quasi steady state is quickly reached for wall temperatures because of its low thermal inertia. Temperatures measured in the central part are plotted along the wall height in figure 2a for maximal solar irradiation (E_s = 845 W.m^{-2}). Cladding temperature varies to small extend between 45 and 55 °C due to the prevalence of solar irradiation on cladding energy balance. Besides, cavity air warms up and its temperature increases from 14 to 46 °C. Due to its low emissivity, radiant barrier temperature is close to cavity air temperature. A similar behavior is observed in the right side of the wall, the temperature difference being always lower than 1 °C compared to the central part.

Measured air velocities are presented in figure 2b. Under natural convection, they vary between 0.1 and 0.25 m.s^{-1}, meaning that air flow is always laminar in the cavity. Their magnitudes depend on cavity design (pressure drop due to friction and local pressure losses) and outdoor boundary conditions (solar irradiation, wind velocity, exterior temperature) and agree with values reviewed by [14]. Velocity measured in the right side of the wall is more noisy and slightly higher than the central part ones. This difference can be due to different positions of hot-wire anemometers in the cavity width where velocity profiles are rather uneven [6]. Here, anemometer located in right part is certainly closer to the cladding. Despite the limitations of velocity measurement with hot-wire anemometers (local measurement, low accuracy at low velocity or disturbance of the flow) [15], the comparison with a mean cavity velocity calculated from volumetric flow rate and cavity cross section is satisfying.

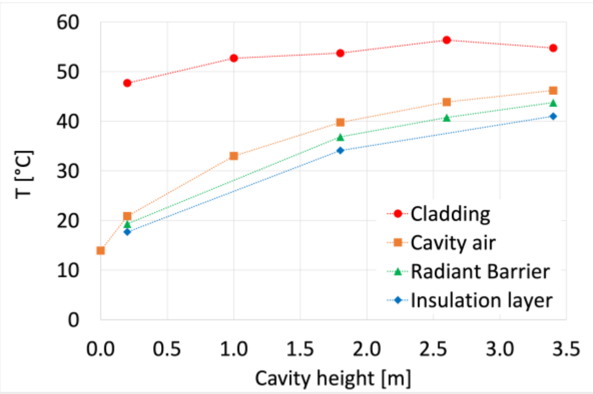

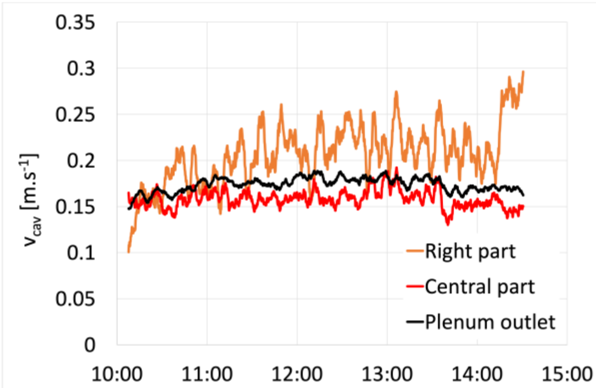

Figure 2. Experimental data measured under natural convection (Exp 1): temperature profiles along the wall height measured at maximal solar irradiation (a) and air cavity velocities (b).

2.3. *Thermal performance analysis*

Considering the opaque ventilated façade as solar air collector, numerous performance indicators are evaluated from experimental data. Heat collected by air in the cavity Q_{col} is given by:

$$Q_{col} = q_v^{air} \rho^{air} c_p^{air} \left(T_{cav}^{out} - T_{cav}^{in}\right) \tag{1}$$

with T_{cav}^{out} and T_{cav}^{in} outlet and inlet cavity temperature, ρ^{air} air density and c_p^{air} air specific heat. Collected energy E_{col} is calculated by integrating collected heat over time. Collector efficiency is defined as:

$$\eta_{OVF} = \frac{Q_{col}}{E_s A} \tag{2}$$

with E_s the incoming total solar irradiation and A the effective area of the façade.

Figure 3 shows their evolution for experiments performed under natural and forced convection. Under natural convection, the temperature difference $\left(T_{cav}^{out} - T_{cav}^{in}\right)$ variation is similar to the solar irradiation ones and reaches a maximum value of 32.5 °C. Since volumetric flow rate is almost constant, collected heat Q_{col} presents also similar variations ranging between 400 and 700 W, with a mean value of 570 W. Considering the uncertainties on air flow rate and temperature measurements, theoretical uncertainty on collected heat Q_{col} is 5 %. Collected energy E_{col} during this experiment is 2.5 kWh. Collector efficiency varies between 9 and 12.75 %, with a mean value of 11 %. Under partly sunny days, air flow rate and cavity temperatures show larger fluctuations due to variable solar irradiation. Even if the thermal inertia of the wall is low, calculated instantaneous collector efficiency show large fluctuations, that should be averaged over several minutes/hours.

Under forced convection, OVF performance depends on flow rate level. Figure 3b displays the results obtained for three imposed flow rates: 61, 118 and 50 m^3.h^{-1}. The higher the flow rate, the higher the heat collected and the higher collector efficiency. Here, a maximal heat flux of 1350 W and a maximal efficiency of 25 % are calculated. Consequently, the mean collector efficiency and the amount of collected energy are higher due to higher mean volumetric flows (see table 1). These results are in agreement with those of [9].

Table 1. Mean weather conditions and mean thermal performance of OVF (NC: natural convection; FC: forced convection).

Experiment	T_{ext} [°C]	E_s [W.m^{-2}]	*Sky cond.*	v_{wind} [m.s^{-1}]	q_v^{air} [m^3.h^{-1}]	T_{cav}^{out} [°C]	η_{OVF} [%]	E_{col} [kWh]
1 – NC	13.00	780	Sunny	1	60	41.7	11.0	2.5
2 – NC	14.16	616	Partly sunny	0.9	53	37.7	10.4	1.8
3 – FC	13.49	504	Cloudy	0.6	57 to 123	31.4	16.5	2.05
4 – FC	12.99	704	Partly sunny	0	50 to 118	42.3	17.6	3

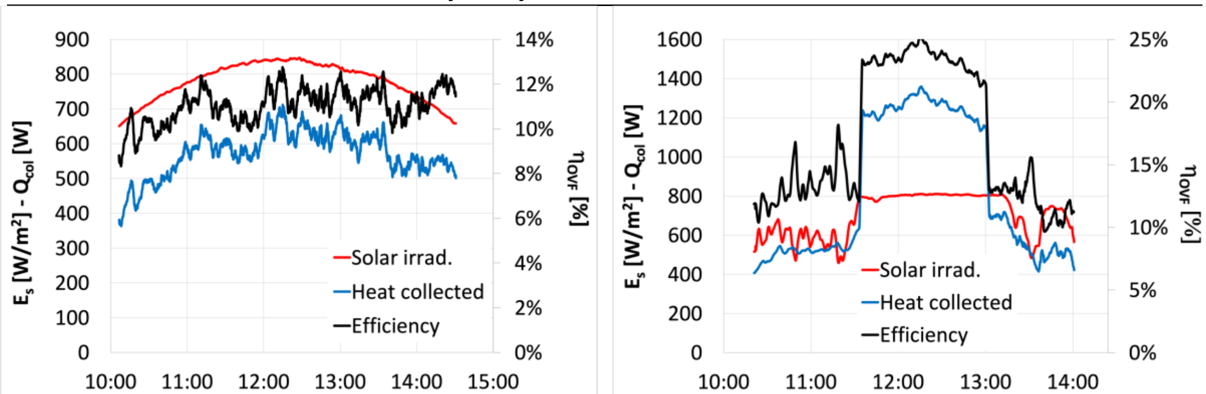

Figure 3. Instantaneous heat collected and collector efficiency calculated under natural convection (Exp 1) (a) and forced convection (Exp 4) (b).

3. OVF modelling

3.1. Model and assumption

OVF modelling requires to cover the following phenomena: absorption of solar irradiation by the cladding; long-wave radiation exchange with the environment; convection with the exterior air; infrared radiation exchange through the air gap; convective exchanges between the air stream and both air gap surfaces; conduction and thermal storage in the internal wall. Numerical modelling approaches reviewed in [16] include CFD, zonal approach or airflow network.

Here, two modelling approaches are compared: the first one is based on Type 1230 provided by Trnsys software and the second one is an internal developed pseudo-2D model. For both models, cladding is supposed to be flat, a mean cavity width of 4 cm is considered, and insulation layer is assumed to be homogeneous over the wall height. Radiative properties are measured in the lab (see table 2). Measured weather data and mass flow within the cavity are used as input. Sky temperature is set to exterior temperature minus 11 °C following the standard ISO 52017. External convective heat transfer coefficient is function of measured wind velocity through the Mac Adams relation:

$$h_{ext}^{conv} = 5.7 + 3.8 v_{wind} \quad (3)$$

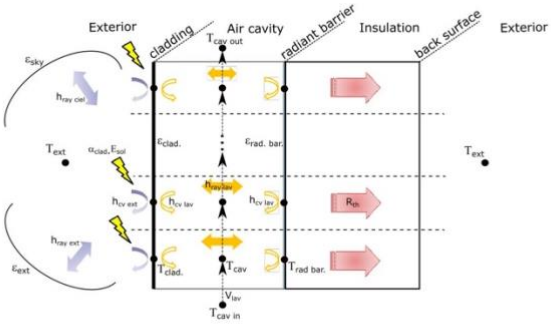

Figure 4. Pseudo-2D thermal model.

Table 2. Measured radiative properties of OVF materials.

	Solar absorptivity	Longwave emissivity
Cladding (ext)	0.96	0.94
Cladding (int)	-	0.83
Radiant barrier	-	0.11

3.1.1. Type 1230. The Type 1230 model is derived from energy balances on the exterior surface, on a cladding including its thermal inertia, on the air stream, and on the back side of the air gap including a massless resistive layer. In this model, Nusselt number is set by the developers to a constant value of 3.66, leading to the unrealistic value of 1 W.m^{-2}.K^{-1} for internal convective heat transfer coefficient whatever air cavity velocity. Long-wave radiation exchanges within the cavity are explicitly solved. The model is solved for a single zone and provides mean surface temperatures and air temperature at cavity outlet. While Type 1230 is usually coupled with Type 56 (Thermal building zone) for simulating the heat transfer across the interior wall [17], it works stand-alone by using the temperature measurement behind the wall.

3.1.2. Pseudo-2D model. A pseudo-2D model was developed by discretizing into 40 nodes along the entire OVF, i.e. air cavity, cladding and insulation layer (see figure 4). Heat transfers in each slice are modelled on the basis of a previous work [18]. Contrary to Type 1230, thermal inertia of the cladding is neglected, and steady state heat balance allows calculating its temperature. Long-wave radiation exchanges from the exterior surface are also considered with the local environment (ground + other buildings supposed to have a temperature equal to the exterior one). Long-wave radiation exchanges within the cavity are linearized and mean measured temperatures are used to calculate radiative heat transfer coefficient. Last, thermal balance in the cavity air accounts for convection, but also for heat provided by the adjacent previous slice. As heat transfers by conduction are not considered along the height of the cladding and insulation layer, the coupling between each node is performed through the air moving inside the cavity. Here, internal convective heat transfer coefficient is changed between 4 and 7 W.m^{-2}.K^{-1} depending on air cavity flow rate [19]. Finally, the model allows evaluating air temperature at cavity outlet, but also all temperature distributions in the vertical direction.

3.2. Comparison with experimental data

Figure 5 and figure 6 present a comparison of temperature variations simulated with Type 1230 and pseudo-2D models with experimental data measured under forced convection. The comparison is done for two sky conditions (partly sunny/Exp4 and cloudy/Exp 3) at various OVF positions. Root mean square errors (RMSE) between simulations and measurements are gathered in Table 3.

Type 1230 model tend to predict the lowest temperature on cladding surface mainly during sunny periods (with differences up to 8 °C) whereas simulated temperature on radiant barrier surface is 4 to 12 °C higher than experimental data. Such differences were also noted by Pergolini et al. [17]. On the exterior surface, simulated long-wave radiation exchanges with the sky are significant whatever the cloud cover, which tends to limit solar heat adsorption. Since internal convective heat transfer coefficient is very small in the cavity, heat is mainly transferred by long wave radiation exchange from the cladding to radiant barrier. Finally, simulated temperature differences between cladding and radiant barrier do not exceed 8 °C instead of 15 °C for experimental data. Despite the low precision of Type 1230 on opaque surfaces, prediction of temperature at cavity outlet are good and RMSE is lower than 2.3 °C.

Pseudo-2D model is more accurate than Type 1230 model during cloudy day, particularly on radiant barrier surface. A good agreement is found for averaged temperatures, but also for locally measured temperatures (not presented in this paper). At the beginning of partly sunny day, large differences (up to 10 °C) are noted in the cladding when solar irradiation is fluctuating significantly: this can be due to the absence of thermal inertia in the cladding model. Nevertheless, these fluctuations are dampened in air cavity outlet and on radiant barrier surface, improving thus the agreement with experimental data. Particularly, setting internal convective heat transfer coefficient as function of air flow rate was found to be necessary to enhance model precision. RMSE was limited to 3.7 °C.

Finally, air temperature at cavity outlet seems to be well predicted with both models. Nevertheless, relative errors up to 9 % are noted on the collected energy, which can lead to collector efficiency overestimation up to 1.5 %. This underlines the challenge of accurate modelling of solar air collector.

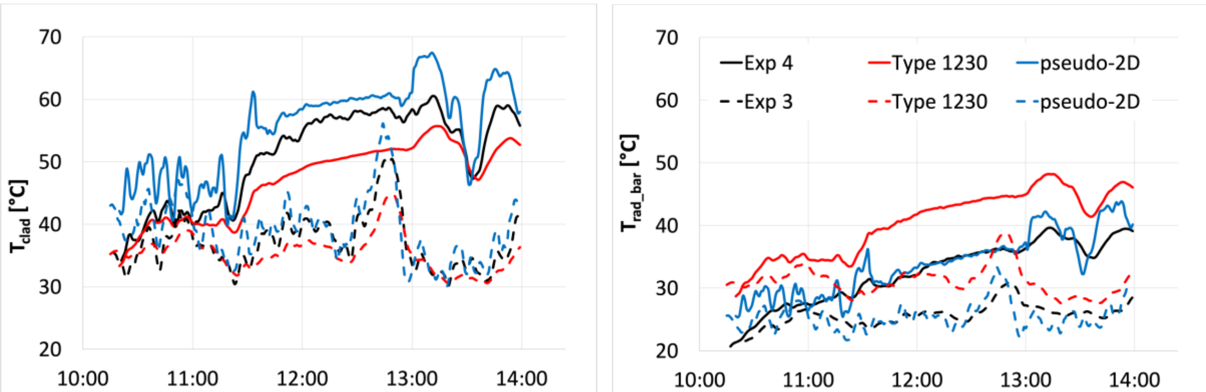

Figure 5. Measured and simulated temperature averaged on cladding (a) and radiant barrier (b) height for OVF working under forced convection for two sky conditions (legend prevails for both graphs).

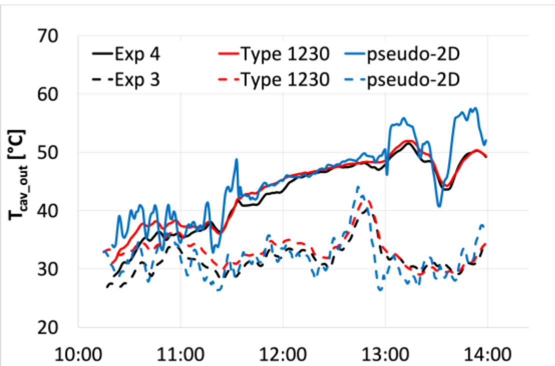

Figure 6. Measured and simulated temperature at cavity outlet for OVF working under forced convection for two sky conditions.

Table 3. RMSE (expressed in °C) for Type 1230 and pseudo-2D models.

		Clad.	Cav. out	Rad. Bar.
Partly sunny	**Type 1230**	4.6	1.4	8.0
	Pseudo-2D	5.2	3.6	2.4
Cloudy	**Type 1230**	2.6	2.3	5.9
	Pseudo-2D	3.3	2.4	2.0

3.3. Sensitivity to alternative design

The sensitivity to two design parameters is investigated: cavity height is changed between 2 and 5 m and radiant barrier Longwave Emissivity (noted LE) is set to 0.7 (which corresponds to longwave emissivity of rainscreen membrane [18]). Their influence on simulated collector efficiency is plotted in figure 7. The higher cavity height, the larger surface subjected to solar radiation, the higher cladding and air temperature at cavity outlet, the higher collector efficiency. Nevertheless, air temperature at cavity outlet converges asymptotically towards a maximum value, since absorbed solar energy is balanced by convective and radiative heat losses. Note that Type 1230 model is less sensitive to cavity height than pseudo 2D since heat balances are averaged over the height and not discretized. For height of 2 or 5 m, the absolute difference on collector efficiency is around 2.5 % between both models.

Radiant barrier longwave emissivity LE has a slight influence on collector efficiency, but a significant influence of its temperature as shown in figure 7b. By increasing LE, radiant barrier temperature increases by 9 °C and cladding temperature decreases slightly by 1.5 °C due to higher longwave radiative exchanges. By means of convective heat transfer, air temperature at cavity outlet increases by 3 °C, which improves the collector efficiency. Since internal convective heat transfer coefficient is lower for Type 1230 model, the effect of LE on collector efficiency is almost negligible.

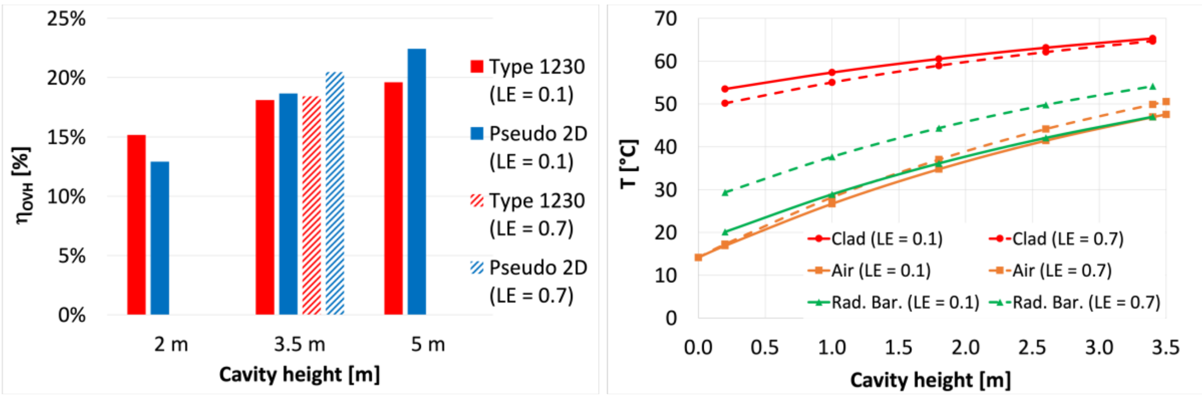

Figure 7. Sensitivity of mean collector efficiency to cavity height and to radiant barrier longwave emissivity (LE) under forced convection (Exp 4) (a) and influence of LE on temperature profiles simulated with pseudo 2D model (b).

4. Conclusions

Air preheating potential with high Opaque Ventilated Façade was evaluated. An experimental set-up was designed to perform tests under natural and forced convection. The instrumentation allowed evaluating temperature fields, air flow rate and, thus, heat exchanges. Results showed that cavity air velocity measured under natural convection is fluctuating and does not exceed 0.2 m.s^{-1}, which leads to low collector efficiency. By controlling air flow, higher amount of energy can be collected.

The experimental data are compared to simulations obtained from two models: Trnsys Type 1230 and home-developed pseudo 2D. Both models could accurately predict air temperature variations at cavity outlet. However, differences were noted in the cladding or in the radiant barrier due to the modelling assumptions. Finally, the models were used to investigate the influence of design parameter on the OVF thermal performance.

References

[1] Ibañez-Puy M, Vidaurre-Arbizu M, Sacristán-Fernández JA and Martín-Gómez C 2017 Renewable and Sustainable Energy Reviews 79 180
[2] Fantucci S, Serra V and Carbonaro C 2020 Energy and Buildings 225 110354
[3] Gagliano A. Nocera F, and Aneli S 2016 Energy and Buildings 122 131
[4] Dimoudi AC, Androutsopoulos AV and Lykoudis SP 2016 Journal of Building Physics 39 297
[5] Stazi F, Vegliò A and Di Perna C 2014 Energy and buildings 69 525
[6] Gagliano A and Aneli S 2020 Solar Energy 205 531
[7] López FP and de Adana Santiago MR 2015 Renewable energy 75 524
[8] Ali MH 2011 Journal of Engineering and Sustainable Development 15
[9] Paya-Marin MA, Lim JB, Chen JF, Lawson RM and Gupta BS 2015 Renewable Energy 83 871
[10] Diallo TM, Zhao X, Dugue A, Bonnamy P, Miguel FJ, Martinez A et al. 2017 Applied energy 205 130

[11] Paya-Marin MA, Roy K, Chen JF, Masood R, Lawson RM, Gupta BS and Lim JB 2020 Renewable Energy 152 799
[12] Nikkerdar F, Rahimi M, Ranjbar AA, Pakrouh R and Bahrampoury R 2021 Energy 220 119781
[13] Gholamibozanjani G and Farid M 2020 Energy 210 118572
[14] Rahiminejad M and Khovalyg D 2021 Building and Environment 190 107538
[15] Giancola E, Sánchez MN, Friedrich M, Larsen OK, Nocente A, Avesani S et al. 2018 Journal of Facade Design and Engineering 6 34
[16] De Gracia A, Castell A, Navarro L, Oró E and Cabeza LF 2013 Renewable and Sustainable Energy Reviews 22 539
[17] Pergolini M, Ulpiani G, Shehi O, Di Perna C and Stazi F 2019 In IOP Conference Series: Materials Science and Engineering 609 032009
[18] Colinart T, Bendouma M and Glouannec P 2019 In MATEC Web of Conferences 282 02014
[19] Suárez C, Joubert P, Molina JL and Sánchez FJ 2011 Energy and Buildings 43 3696.